Multivariable Control in a Critically Loaded Compressor Cascade

Olaf Wiederhold[1], Martin Hecklau[2], Rudibert King[1], Wolfgang Nitsche[2], André Huppertz[3] and Marius Swoboda[3]
[1]Chair of Measurement and Control, Berlin Institute of Technology, olaf.wiederhold@tu-berlin.de
[2]Chair of Aerodynamics, Berlin Institute of Technology, martin.hecklau@tu-berlin.de
[3]Rolls-Royce Deutschland Ltd. & Co. KG, andre.huppertz@rolls-royce.com

Abstract

An experimental study of a closed-loop multiple-input multiple-output (MIMO) control strategy is presented to mitigate flow separation in a compressor cascade. As a result of the highly loaded stator blades a complex three dimensional flow field develops. Concomitantly, flow separation occurs both at the sidewalls and on the suction side of the blades. In order to suppress separation, methods of active flow control are applied. To detect the flow separation phenomena, adequate surrogate variables can be identified by means of PIV measurements. The effect of pulsed blowing through slit nozzles on the sidewalls and the stator blade is evaluated. A multivariable robust H_∞-approach is shown to control the separation phenomena simultaneously. Based on a dynamic decoupling, a classical inverse-based controller (IBC) is even capable of controlling the dominant vortex structures in a decoupled manner. To demonstrate the robustness of the applied methods experimentally, heavy disturbances are simulated. By rejecting them the proposed control algorithms guarantee stable operating conditions. As a result, the performance of the cascade can be significantly increased by means of active flow control.

1. INTRODUCTION

Active flow control has proven its enormous capacity in improving technical processes regarding safety, noise, pollution or energy efficiency. The possibilities of active flow control (AFC) have been investigated for a long time and a wide variety of different approaches have been proposed. Excellent overviews are given by (Gad-el-Hak, et al. 1998) or (Fiedler and Fernholz 1990). Applications of AFC range from the drag reduction of a bluff body (Beaudoin, et al. 2006) or the lift enhancement of an airfoil (Heinz, et al. 2010) to combustion control (Paschereit, et al. 2000), to mention just a few examples. Flow control is by no means restricted to simple setups as surveys on helicopters (Nelson, et al. 2000), civil aircrafts (McLean, et al. 1999) or turbomachines (Culley, et al. 2004) demonstrate. Due to the high complexity of a turbomachine the application scenario of active flow control technology is manifold and the potential seems enormous as (Tavakoli, et al. 2004), (Lord, et al. 2000) or (Day, et al. 1999) point out in their surveys considering gas turbines, compressors and commercial jet engines, respectively. In axial compressors, as they are used in gas turbines and jet engines, the performance is limited by a variety of different instabilities caused by flow separation. Since a certain safety margin to the stall boundary has to be guaranteed, the engine cannot be run at its optimal operating point (Walsh and Fletcher 1998).

In order to improve the performance of axial compressors the majority of studies focus on rotor instabilities and boundary layer separation on the rotor blades or instabilities of the whole compression system (Inoue and Kuroumaru 1989), (Epstein, et al. 1989), (Eveker, et al. 1998). In contrast, the present investigation deals with a compressor cascade with critically loaded stator blades. By increasing the turning angle of the single stator blades the achievable pressure ratio per compressor stage can be enhanced. As a result, the same overall pressure ratio could be reached with less compressor stages. Likewise, the total weight and size of a compressor could be reduced.

However, by increasing the critical loading of the blades, flow separation might arise accompanied by complex three dimensional flow fields, see (Langston 1980), (Nerger, et al. 2007), (Hecklau, et al. 2010c). The formation of secondary flow structures at the sidewalls and a pressure induced flow separation on the suction side of the stator blades lead to significant aerodynamic losses (Hecklau, et

al. 2010b), (Gmelin, et al. 2010). Methods of active flow control are proposed here to prevent boundary layer separation and enable an overcritical turning. In contrast to passive means like vortex generators, guide vanes or other permanent geometric modifications, active control is able to react to a change in operating conditions and compensate for unexpected disturbances immediately.

In this study pulsed blowing through slit actuators at the sidewalls and on the blades is used to alleviate flow separation. As a result of the complex three dimensional flow field and the available actuator setup, an appropriate multiple-input multiple-output controller design is necessary (Skogestad and Postlethwaite 2005).

Two different control strategies are used here. To mitigate flow separation a H_∞-method is proposed (Kwakernaak 1993). This control approach is employed for example by (Nelson, et al. 2000) in a single-input multiple-output (SIMO) experiment to stabilize surge in a turboshaft engine. (Weigl and Paduano 1997) show that a constant gain controller is not sufficient to handle compressibility effects within a transonic compressor and propose instead a H_∞-control. In this work a multivariable H_∞-controller is shown to be capable of simultaneously mitigating both dominant separation phenomena. Additionally, a classical approach based on a dynamic decoupling of the plant model in combination with an integrating controller (IBC) (Skogestad and Postlethwaite 2005) is proposed which even enables a decoupled influence of the vortex structures.

Both control strategies are investigated experimentally with respect to their robustness by simulating heavy disturbances in the system.

This paper is organized as follows: The experimental setup, the base flow field and the derivation of suitable surrogate control variables are reviewed in Chapter 2. The controller synthesis concerning both control strategies is described in Chapter 3. The obtained results are presented in Chapter 4 followed by an outlook and a conclusion in Chapter 5.

2. EXPERIMENTAL FACILITY

2.1. Cascade Test Rig

All experiments are performed in a low-speed cascade test rig at the Chair of Aerodynamics. The stator compressor cascade consists of seven blades, as shown in Figure 1. The cascade and stator geometry (cf. Table 1) is provided by Rolls-Royce Deutschland. The blades are designed with an overcritical turning and a low aspect ratio of $AR = 0.8$. In order to change the aerodynamical loading of the blades by variation of the inflow angle, the cascade is mounted on rotatable disks. A homogeneous cascade inlet flow is achieved by two additional tailboards and boundary layer suction at the end of the horizontal endwalls. At each sidewall 14 static pressure taps are installed for monitoring the inlet flow uniformity.

The cascade test rig is operated in an open wind tunnel. Corresponding to the design Mach number of $Ma = 0.1$ and a constant total temperature of $T_{t,1} = 294$ K the velocity at the inlet is $u_1 = 34$ m/s. Based on the blade chord length, the Reynolds number is $Re_L = 8.4*10^5$. The inflow turbulence intensity is $Tu = 2.1\%$.

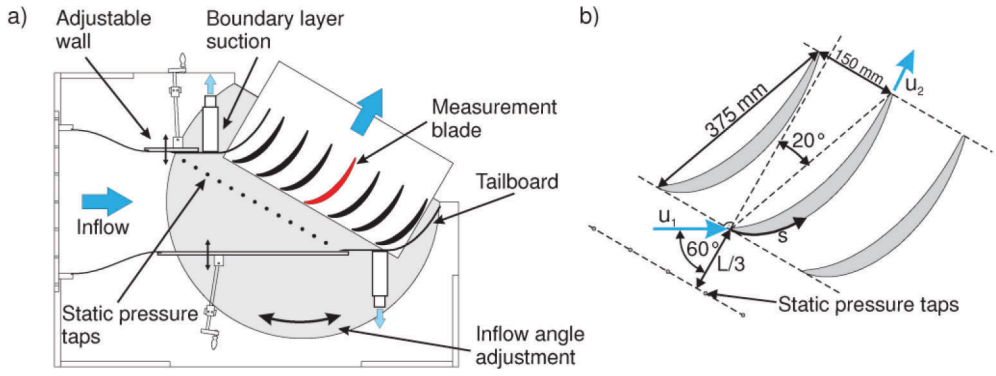

Figure 1. a) Cascade test rig; b) Stator blade geometry, (Hecklau, et al. 2010b).

Table 1. Characteristics of test rig.

Quantity	Value
Chord length L	0.375 m
Blade height h	0.3 m
Aspect ratio h/L	0.8
Pitch to chord ratio t/L	0.4
Stagger angle γ	20°
Inflow angle β	60°

2.2 Base Flow

Due to critical loading of the stator blades, the low aspect ratio, and the high flow turning of the blades, a fully three-dimensional flow field with boundary layer separation is developing. Figure 2 shows the complex flow topology within the passage.

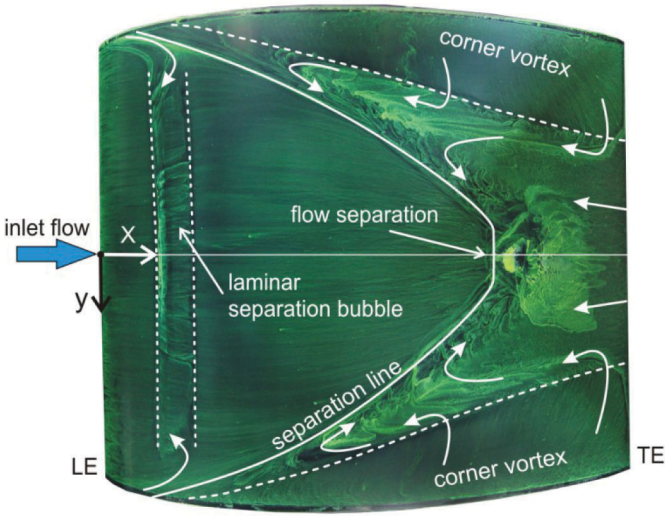

Figure 2. Oil-flow visualization of the stator blade's suction surface, (Hecklau, et al. 2010c).

The oil flow visualization on the blade suction surface illustrates the corner vortex formation and the three-dimensional separation line. The general observed flow pattern is as follows: The laminar boundary layer separates towards the front of the blade suction side surface, forming a laminar separation bubble. The separated flow undergoes transition, reattaching on the blade suction surface as a turbulent boundary layer (Burgmann and Schröder 2008). At the streamwise position of the turbulent reattachment, secondary flows caused by the endwalls come into effect. The main flow is narrowed in streamwise direction. Between the secondary and the main flow, a three-dimensional separation line is formed, ending up at midspan, where separation nearly perpendicular to the main flow occurs.

2.3 Actuation

Sidewall Actuator: As shown in Figure 3 in red colour, pulsed blowing of compressed air out of the cascade sidewalls is used to control the dominant secondary flow structures. Therefore, the air is blown through rectangular slots. The slots have a height of 20 mm and a width of 0.4 mm. The angle of the injected air to the sidewall is 15° in the main flow direction and the actuator is located at 10% of the blade's chord length. The sidewall actuator setup for 6 blades consists of 12 solenoid valves which are directly connected to the actuator chamber. The actuator chamber decelerates the compressed air flow and converts the circular cross section of the pressure pipe to the rectangular actuator slot. For symmetrical flow conditions during actuation, all passages of the cascade are equipped with actuators on both sidewalls.

Blade Actuator: The flow separation at the rear part of the blade is suppressed by actuators installed inside the stator blades. The blade actuators are integrated with the solenoid valves in the stator blades. Each slot-segment, cf. Figure 3 in cyan colour, is equipped with one solenoid valve, which can be

operated individually. Between the segments the distance is kept as small as possible, resulting in a separation of 2 mm. The slots are orientated in spanwise direction with a geometry of 50 mm in length and 0.4 mm in width. The wall jet has an angle of 45° to the local blade surface. Due to the shape of the actuator cavity, an almost uniform velocity distribution in span-wise direction is obtained (Hecklau, et al. 2010b). For the closed-loop control experiments shown here the three segments are used as one actuator device.

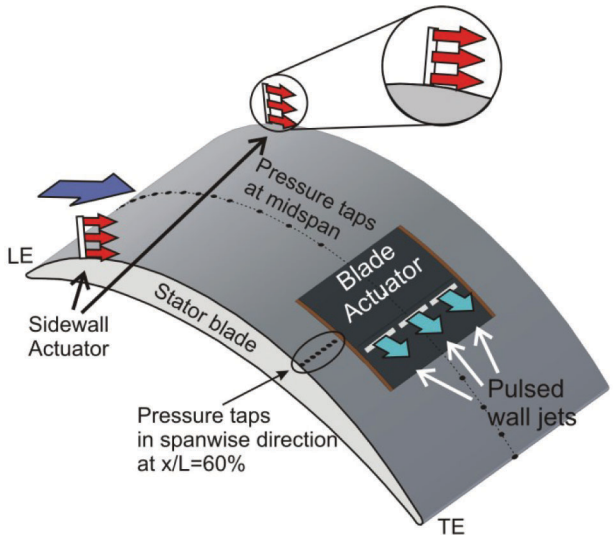

Figure 3. Actuator setup and instrumentation of a stator blade, adapted from (Hecklau, et al. 2010a).

Fast-switching solenoid valves (Festo MHE2, with a switching frequency up to 250 Hz) are used for pulsating the compressed air in both actuator concepts. The mass flow of air passing through the actuators is measured by a mass flow meter (Bronkhorst F-203AC, accuracy 1%).

The actuation amplitude is controlled by pressure control valves (Festo, MPPE) adjusting a certain pressure level p_d in a pressure distributor which in turn provides the actuating valves with air. A look-up table, cf. Figure 4, shows the injected mass flow of the actuators at the sidewall (sw) and on the blade (ba) per passage, i.e., two actuators at the sidewall and three at the blade. The values are given as functions of the adjusted pressure level in the distributors. Here, the injected actuator mass flow $\dot{m}_a$ is normalized by the actual passage through flow $\dot{m}_{pas} \approx 0.93$ kg/s and the pressure within the distributor p_d is referred to its maximal value of $p_{d,max}$ = 6 bar. The corresponding actuator frequencies used are $f_{act,sw}$ = 120 Hz and $f_{act,ba}$ = 40 Hz.

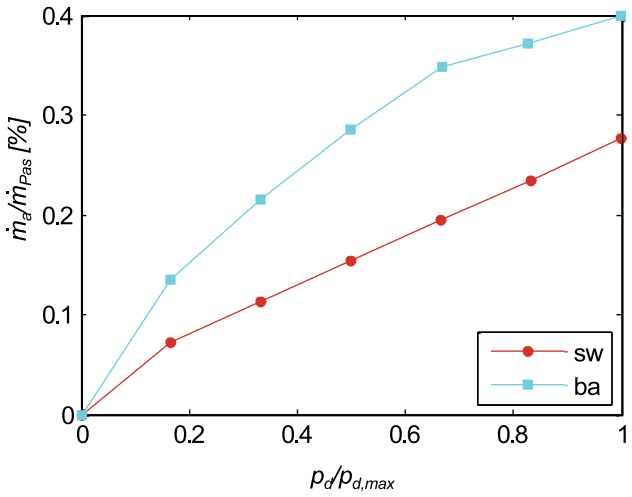

Figure 4. Injected mass flow rates of the actuators at the sidewall (sw) and on the blade (ba) as a function of the supplied distributor pressure p_d, with $p_{d,max}$ = 6 bar.

The centre stator blade of the cascade is equipped with static pressure taps on the suction and pressure side, cf. Figure 3. The local static pressure p_x along the blade's surface at discrete positions can be quantified. Fast responding miniature differential pressure sensors (SensorTechnics, RMOH) are placed directly below the blade's surface. The frequency response of the pressure sensors in combination with the pressure taps is constant up to 500 Hz. The non-linearity and hysteresis for this sensor is ±0.25% of the full span scale. For the setup used measuring the pressure distribution c_p along the blade, a maximal uncertainty of +-0.7% results. Along the midspan of the stator blade 30 pressure taps are installed, 19 taps placed on the suction side, 10 on the pressure side and one pressure tap on the trailing edge (TE) of the blade. Additionally, static pressure taps are placed at x/L = 60% of the chord length in spanwise direction. All static pressure information is measured simultaneously with a digital signal processor (DSP), as it is indicated in Figure 5. The static pressure of the inlet velocity p_1 is used as the referential pressure of the static pressure measurements $p_x - p_1$ and the static pressure coefficient is calculated by

$$c_p = (p_x - p_1) / q_1 \tag{1}$$

with q_1 denoting the dynamic pressure of the flow.

Digital Signal Processor (DSP): In order to perform closed-loop control experiments, a DSP is employed (dSpace controller board DS 1005, A/D converter board DS 2003, D/A converter board DS 2103). This system enables the online signal processing of the measured data, the calculation of a control signal and the generation of the signals for the jet actuators in real-time, cf. Figure 5.

For the ease of understanding the underlying control architecture is indicated in the block diagram in Figure 6, where a so-called cascaded control structure can be seen. Here, s denotes the Laplacian variable.

The applied control pursues mainly two aims: The first is to drive the system accurately to desired reference commands $r(s) = y_{desired}(s)$. Furthermore, it is required to reject disturbances $d(s)$ acting on the system effectively. Both tasks are realized by the controller $\mathbf{C}_2(s)$ in the outer loop. Depending on the actual control error $e(s) = r(s) - y(s)$ the controller $\mathbf{C}_2(s)$ determines the necessary pressure levels in the distributors $\mathbf{G}_1(s)$.

For this, classical PI-controllers $\mathbf{C}_1(s)$ are used in an inner control loop. The bandwidth of this inner control loop is higher (2-10) than the one of the outer loop. For $\mathbf{C}_2(s)$ the inner loop is a part of the overall dynamic of the plant.

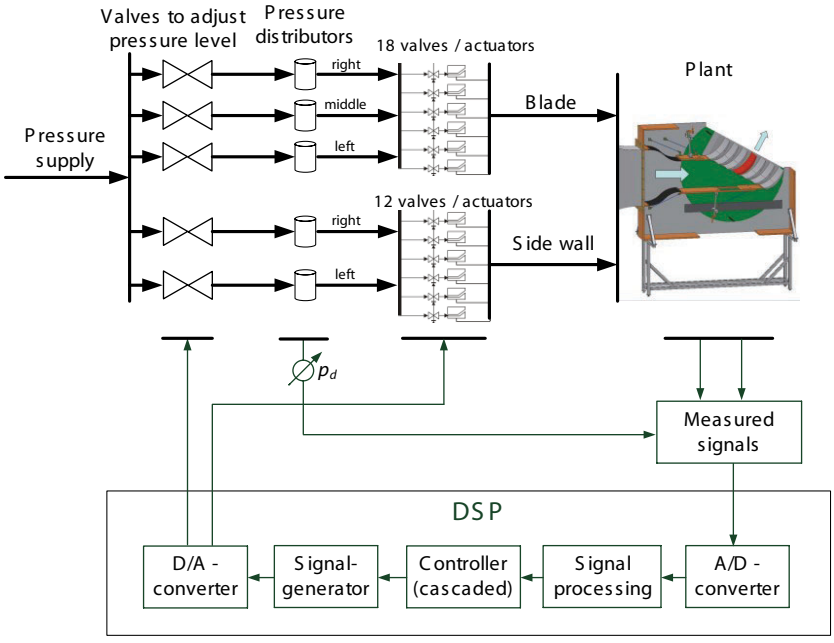

Figure 5. Schematic diagram for signal flows in closed-loop control experiments.

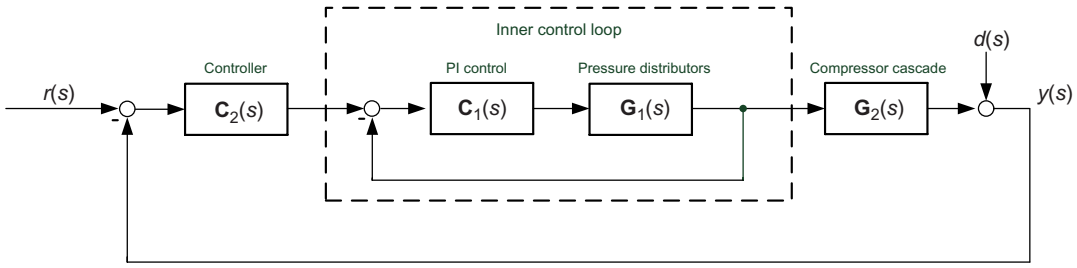

Figure 6. Block diagram of the cascaded MIMO-control architecture.

2.4 Derivation of surrogate control variables

In order to influence the above described dominant separation phenomena by means of closed-loop control it is essential to identify suitable surrogate control variables which represent the actual flow state in an appropriate manner. These variables have to be accessible in real-time and easy to measure to be applicable in a real engine in the long run.

Two surrogate control variables are introduced which fulfil the required prerequisites, namely a spanwise pressure difference $\Delta c_{p,spw}$ measured at a chord length of x/L = 60% and the rise in pressure at the trailing edge $\Delta c_{p,TE}$.

A motivation for the first value is given by the stereoscopic PIV-records presented in (Hecklau, et al. 2010c). As reported the corner vortices get pushed to the sidewalls with the use of the side-wall actuator and the blockage of the passage flow is reduced concomitantly. Hence, a reduction of the passage blockage is obtained. This results in a decreased total pressure loss, as well as in an increased turning across the passage of the compressor cascade. Furthermore, the position of the corner vortex unambiguously correlates with the spanwise pressure distribution. The spanwise pressure distribution at x/L=60% is depicted in Figure 7. It can be observed that in the case of actuation, i.e., with a shifted corner vortex, a much flatter pressure profile is obtained giving rise to a smaller spanwise gradient. Exploiting this, the position of the corner vortex can be estimated. Therefore the pressure information of the sensors at 47%, 44%, 41% and 38% of the blade span are used to derive a control variable. A spanwise pressure difference Δc_p is defined as follows:

$$\Delta c_p = (c_{p,47} - c_{p,44}) + (c_{p,47} - c_{p,41}) + (c_{p,47} - c_{p,38}) \tag{2}$$

Accordingly, the control variable $\Delta c_{p,spw}$ is defined as the difference between the actuated case $\Delta c_{p,act}$ and the base flow case without actuation $\Delta c_{p,0}$:

$$\Delta c_{p,spw} = \Delta c_{p,act} - \Delta c_{p,0} \tag{3}$$

Regarding the applicability within real jet engines it has to be noted that the same qualitative signal is obtained by exploiting only the sensor information at the positions 47% and 38% blade span. However, using four sensors leads to a less noisy signal.

In order to acquire another suitable control variable, a pressure distribution at the midspan of the suction side of a stator blade is shown in Figure 7. The averaging period is Δt = 5s. By injecting air through the blade actuators the pressure-induced boundary layer separation can be delayed and the turning of the blade rises substantially. Due to the increased turning, the diffusion through the stator passage is enhanced. This results in a static pressure rise $\Delta c_{p,TE}$ which can be unambiguously observed at the trailing edge of the blade as indicated in Figure 8. Hence, this pressure information seems to be a suitable parameter for the use as another control variable because it represents an important global aspect of the actual flow state. Moreover, it is easy to measure by only one pressure sensor at the trailing edge.

For the realization of the closed-loop control experiments both control variables, $\Delta c_{p,TE}$ and, $\Delta c_{p,spw}$ fulfil the most important prerequisite of real-time accessibility. Averaging times of Δt = 0.05s are sufficient to obtain signals suitable for closed-loop control.

Further detailed information about the flow physics within the stator cascade can be found in previous numerical and experimental investigations such as (Hecklau, et al. 2010b) or (Gmelin, et al. 2010).

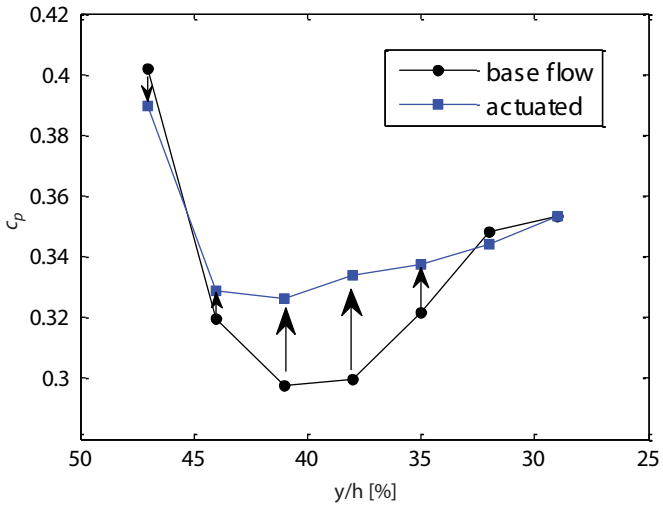

Figure 7. Spanwise pressure distribution at x/L = 60% for the base flow and the actuated case. Pulsed blowing is used at the sidewall actuators with a forcing frequency of $f_{act,sw}$= 120 Hz, a fixed duty cycle of DC = 50% and actuation amplitude of $(p_d/p_{d,max})_{sw}$ = 0.5.

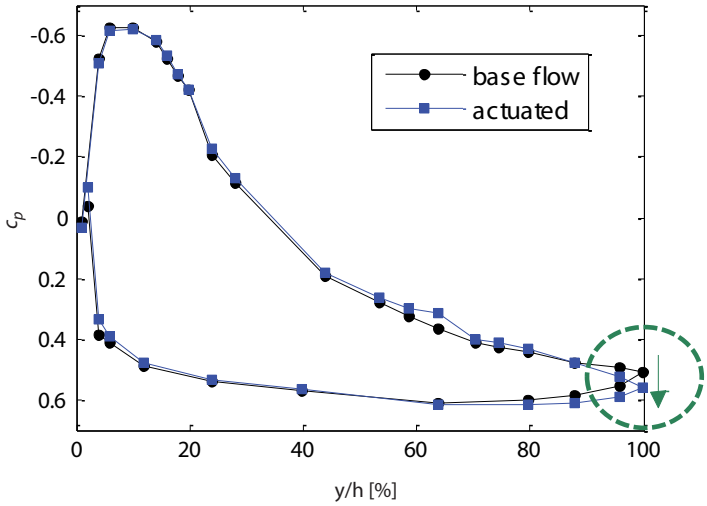

Figure 8. Pressure distribution at midspan x/h = 0% for the base flow and the actuated case. Pulsed blowing is used at the blade actuators with a forcing frequency of $f_{act,ba}$ = 40 Hz, a fixed duty cycle of DC = 50% and actuation amplitude of $(p_d/p_{d,max})_{ba}$ = 0.67. The circle indicates the pressure rise at the trailing edge.

The static influence of both the blade and the sidewall actuators on the two control variables is summarized in look-up tables visualized in Figure 9. The characteristics are recorded with an averaging time of Δt = 5s. The actuation is given in a normalized way, cf. Figure 4. The corresponding frequencies are chosen to be $f_{act,sw}$ = 120 Hz and $f_{act,ba}$ = 40 Hz as they are applied in the following closed-loop experiments. The actuator frequencies are chosen with respect to the strongest effect on the derived control variables. However, it remains part of ongoing research which set of parameters has the best effect on the main flow. Investigations with different actuation frequencies as well as steady blowing can be found in (Hecklau, et al. 2010a), (Zander, et al. 2009) or (Mertens, et al. 2008).

The upper plots in Figure 9 show the impact of the blade as well as the sidewall actuators on the gain in static pressure at the trailing edge $\Delta c_{p,TE}$. Both cause a significant rise, though the influence of the blade actuator is stronger. Referred to the base flow case an increase of about 6% and 13% pressure rise, respectively, is attainable with full amplitude actuation. Regarding the $\Delta c_{p,TE}$-curve under the influence of the sidewall actuation it is noted that the curve obviously shows a higher sensitivity for certain lower actuation amplitudes and then becomes more insensitive starting from $(p_d/p_{d,max})_{sw} = 0.33$.

The assumption at this point is that a certain amount of actuation energy is necessary before the corner vortex finally bends towards the sidewall. This explanation is corroborated by inspection of the values of the spanwise pressure coefficient $\Delta c_{p,sw}$ as illustrated in the lower plot of Figure 9 b).

As explained above, cf. Figure 7, the spanwise pressure distribution gets flatter which results in a decrease of $\Delta c_{p,spw}$. At first, for low actuation amplitudes $(p_d/p_{d,\max})_{sw} < 0.17$ the corner vortex is affected weakly. Then the curve shows its steepest descent between $(p_d/p_{d,max})_{sw} = [0.17\ 0.33]$ indicating that the corner vortex bends towards the sidewall. Finally, for increasing actuation amplitudes the corner vortices get pushed continuously closer to the walls. By this, the blockade of the passage through flow is reduced and the pressure at the trailing edge rises as well.

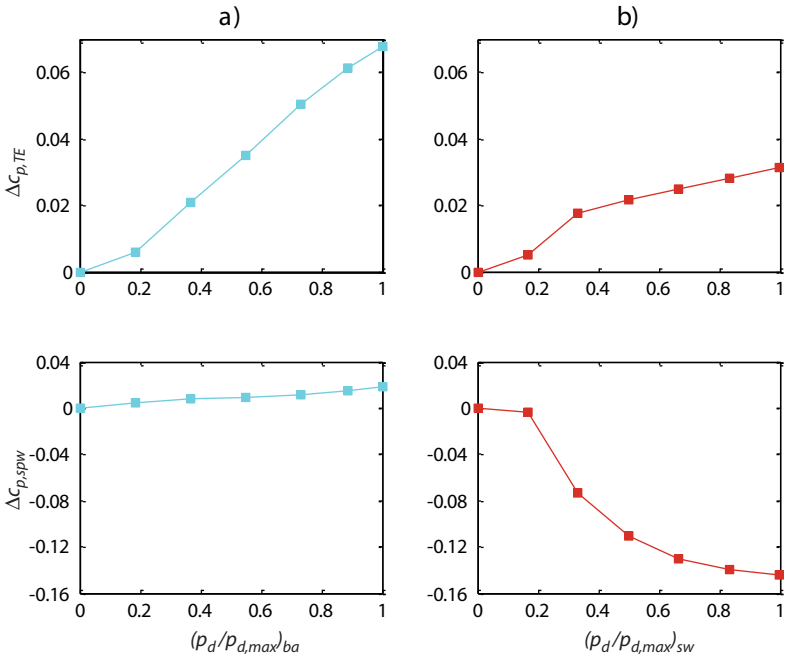

Figure 9. Open-loop characteristics of the surrogate control variables as functions of the applied actuation at the blade (ba) and at the sidewall (sw).

Compared to the influence of the sidewall actuators the impact of the blade actuators on the spanwise pressure difference $\Delta c_{p,spw}$ is almost negligible which is evident from the geometric positions of the spanwise pressure sensors and the blade actuator. However, with high amplitudes the blade actuator has a small negative effect on the spanwise pressure distribution. By injecting air into the boundary layer through the blade actuators the pressure induced flow separation is mitigated. At the same time the whole passage flow rises and the corner vortices get pulled towards mid-span by which $\Delta c_{p,spw}$ increases.

The unambiguous correlation between the control variables indicates the coupled complex flow physics within the cascade flow. Hence, the stator cascade exploiting two actuators consists of a coupled multiple-input multiple-output process for which an appropriate control approach is needed. For clarification a schematic view of the MIMO-control task is shown in Figure 10. The thicknesses of the arrows indicate the influence upon the control variables. The broken black line limits the area of expansion of the corner vortices, cf. Figure 2.

For the sake of completeness it has to be mentioned that for the actuation parameters tested a combined use of both actuators at the same time results in a linear superposition of the characteristics shown in Figure 9. However, nonlinear actuator effects are observable by a combination of steady and pulsed blowing. As this aspect is not in the focus of this paper the interested reader is referred to (Hecklau, et al. 2010a) and (Hecklau, et al. 2010b).

3. CLOSED-LOOP CONTROL

In order to control both dominant separation phenomena simultaneously two different MIMO-control strategies are pursued. The first approach is a classical MIMO-control method based on a dynamic decoupling in combination with an integrating controller, see e.g. (Skogestad and Postlethwaite 2005).

The second proposal is a robust control approach, namely the well known H_∞-control (Kwakernaak 1983). For uncertain systems H_∞-control guarantees stability even for the worst' identified plant model which is used to describe the process. Furthermore, performance criteria can be included readily.

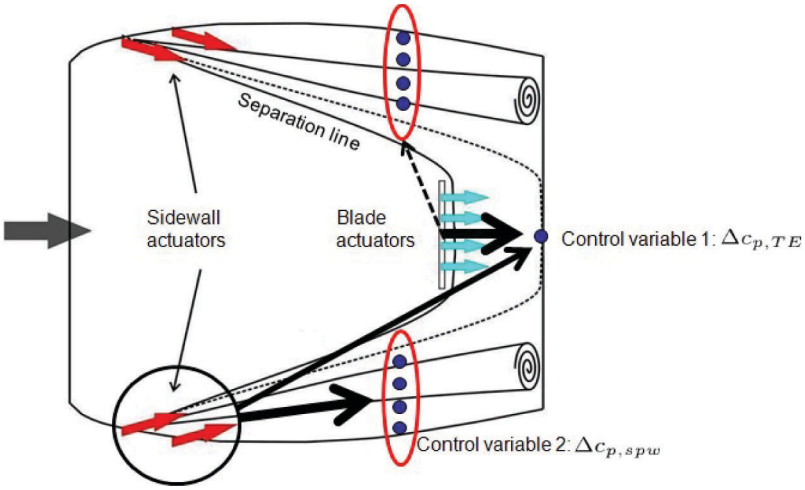

Figure 10. Depiction of the multiple-input multiple-output control scheme, adapted from (Hecklau, et al. 2010a).

Profound knowledge about a plant allows for good control results. The physics of a complex process, however, can never be completely described by a mathematical model. Moreover, in real applications, the control will always have to face immeasurable disturbances. Additionally, for the controller synthesis, a simple model is often preferred to avoid an unnecessary complex model-based control law. Such laws could lead to a high sensitivity of the overall approach and may result in a significant reduction of the control performance.

3.1 System dynamics and determination of a nominal design model

For determining a nominal process model $\mathbf{G}_n(s)$ and the spread of the uncertain system parameters experimentally, a series of representative experiments with stepwise changes of the inputs are conducted. By that, a family Π of perturbed of black-box models $\mathbf{G}_p(s)$ is identified which describes the nonlinear behaviour of the real process by local linear models. The 2 × 2 transfer matrix $\mathbf{G}_p(s)$ consists of four SISO-transfer functions relating all control inputs with all outputs.

For this purpose both control input variables $u_{ba} = (p_d/p_{d,max})_{ba}$ and $u_{sw} = (p_d/p_{d,max})_{sw}$ as well as the process outputs $\Delta c_{p,TE}$ and $\Delta c_{p,spw}$ are considered at the same time. One selected example of a representative experiment is shown in Figure 11.

At the lower panel the control inputs are shown which vary in a stepwise manner to 50% of their maximal values. First, the amplitudes of the blade actuators are activated three times after each other for 10s every pulse. Afterwards three step-up/step-down commands of the sidewall actuators follow. The corresponding measured system response can be seen in the two upper panels of Figure 11 in black colour. Additionally, the simulation of an identified MIMO-process model is shown in a green broken line. In comparison, both characteristics match quite well, indicating that the model is capable of describing the essential behaviour of the process appropriately. For the identification, a commercial MATLAB routine (The MathWorks 1997) is exploited that uses prediction error methods (Zhu 2001). The substantial dynamic behaviour of the output value can be approximated by simple stable linear black-box models $\mathbf{G}_n(s)$ $\mathbf{G}_p(s)$ of second order for all four SISO-transfer functions, i.e., transfer functions of the form

$$G_{p\,ij} = \frac{b_0 + b_1 s}{a_0 + a_1 s + a_2 s^2}$$

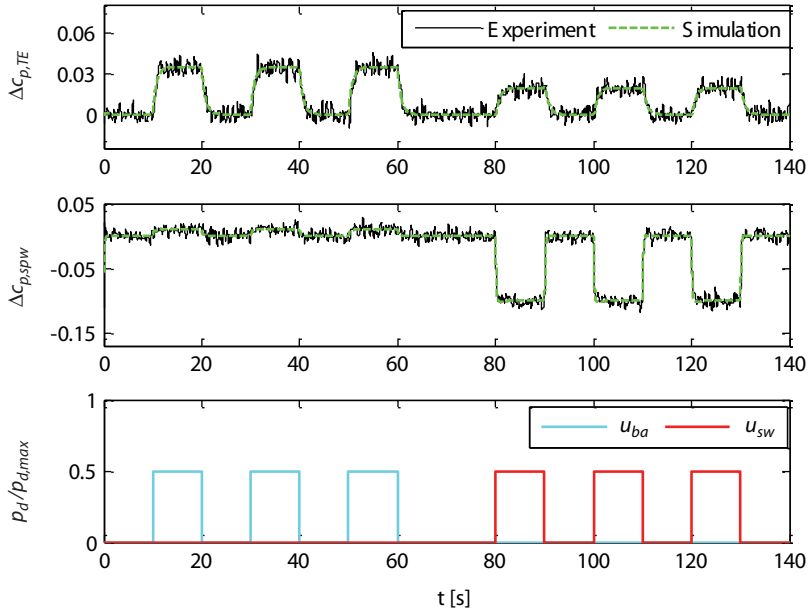

Figure 11. Example of a multivariable experiment for identification.

Frequency responses of all identified black-box models are given in Figure 12 by their minimal and maximal singular values $\underline{\sigma}$ and $\bar{\sigma}$ (Skogestad and Postlethwaite 2005). By means of these a linear nominal model $\mathbf{G}_n(s)$ is derived. Moreover, the amplitude of a multiplicative uncertainty description $1_M(\omega)$ is calculated as follows:

$$1_M(\omega) = \max_{G_p \varepsilon \prod} \bar{\sigma}((\mathbf{G}_p(j\omega) - \mathbf{G}_n(j\omega))\mathbf{G}_n(j\omega)^{-1}) \tag{4}$$

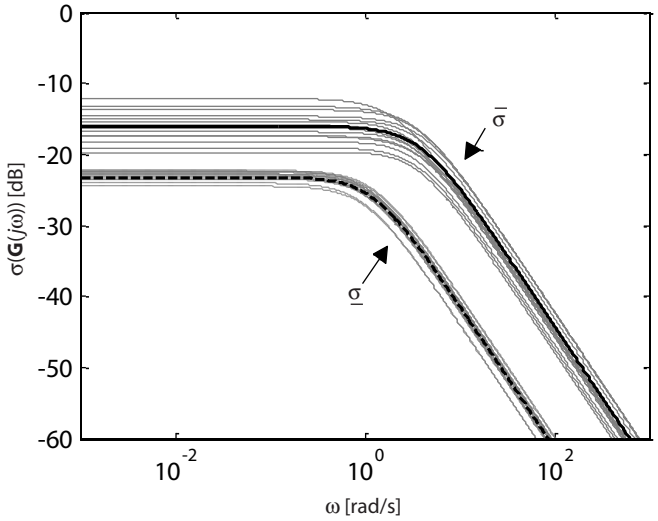

Figure 12. Family of all identified black-box models and a nominal MIMO-model (thick solid and broken line).

The value $1_M(\omega)$ serves as a measure for the uncertainty of the nominal model and therefore can be interpreted as the validity range of $\mathbf{G}_n(s)$. It is used for the H_∞-controller synthesis. More details about the design process of a robust controller are given after the following description of an inverse-based controller.

3.2 Inverse-based controller (IBC)

With an IBC a classical multivariable control strategy is pursued. At first a compensation of the internal coupling is accomplished and then, if successful, a completely decoupled extended plant is controlled by decoupled standard controllers as for example PI-controllers. Thus, the controller matrix without the decoupler usually has only entries on its diagonal. Due to the relative simple model structure of the

identified nominal model $\mathbf{G}_n(s)$, cf. chapter 2, a complete dynamical decoupling is possible in our case. The decoupler is obtained from an inversion of the MIMO-nominal model

$$\mathbf{W}_1(s) = \mathbf{G}_n^{-1}(s) \tag{5}$$

To control the extended plant $\mathbf{G}'(s) = \mathbf{G}(s)\mathbf{W}_1(s)$, cf. Figure 13, decoupled integrators are applied. The overall controller is given by:

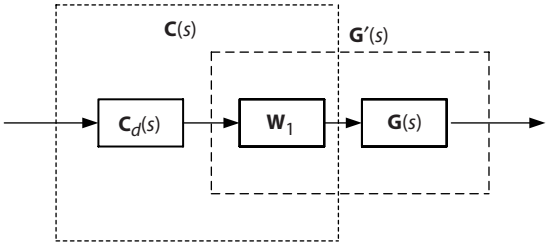

Figure 13. Schematic setup of an IBC.

$$\mathbf{C}(s) = \mathbf{W}_1(s)\mathbf{C}_d(s) = \mathbf{W}_1(s)\mathbf{I}\frac{1}{\mathbf{T}_I s} = \mathbf{W}_1(s)\frac{1}{\mathbf{T}_I s} \tag{6}$$

In Equation (6) $\mathbf{W}_1(s)$ does not need to be realizable, but $\mathbf{W}_1(s)\mathrm{C}_d(s)$. The value of the time constant is chosen in between the bandwidths of the two control variables as $T_I = 0.33$s, cf. Figure 11 and 12, respectively. The σ-plots of the corresponding multivariable controller $\mathbf{C}(s)$ is shown in Figure 14. Additionally, the singular value of the open-loop transfer function $\mathbf{L}(\mathrm{s}) = \mathbf{G}_n(s)\mathbf{C}(s)$ and the complementary sensitivity $\mathbf{T}(s) = \mathbf{L}(s)(\mathbf{I} + \mathbf{L}(s))^{-1}$ can be seen. The frequency response of the controller decreases with 20 dB per decade in the range of low frequencies and remains constant afterwards resembling the behaviour of PI-controllers. The spread of $\underline{\sigma}(\mathbf{C}(s))$ and $\bar{\sigma}(\mathbf{C}(s))$ is a result of the different dynamics of the plant.

The diagram of the open-loop transfer function $\mathbf{L}(s)$ shows a continuous decay of 20 dB per decade throughout the whole frequency range which is supposed to provide for a good disturbance attenuation and a disappearing tracking error with respect to constant reference commands. The bandwidth of $\underline{\sigma}(\mathbf{L}(s))$ and $\bar{\sigma}(\mathbf{C}(s))$ have values of $\underline{\omega}_c = 6$ rad/s and $\bar{\omega}_c = 16$ rad/s, respectively. This indicates an acceleration of the system dynamics by the applied controller. Moreover, the frequency response of the complementary sensitivity function $\mathbf{T}(s)$ indicates a good setpoint tracking in the range of active control, i.e., in the range of lower frequencies.

In the following a robust control approach is presented as an alternative to this control strategy.

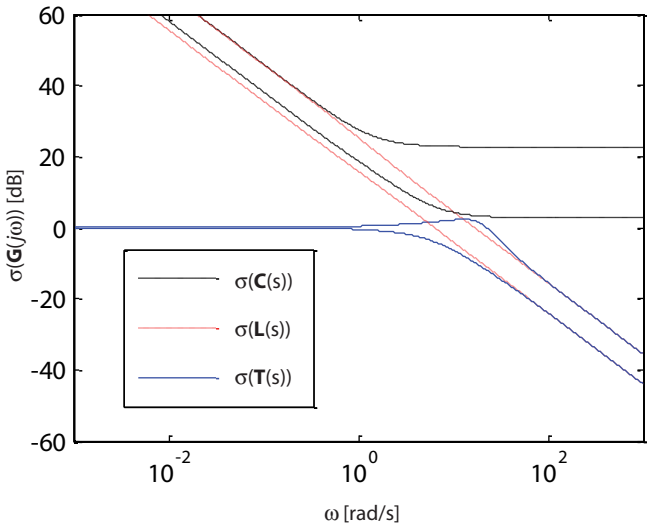

Figure 14. Singular values of the IBC $\mathbf{C}(s)$, the open loop transfer function $\mathbf{L}(s)$ and the complementary sensitivity transfer function $\mathbf{T}(s)$.

3.3 Multivariable H_∞-control

In order to synthesize a multivariable H_∞-controller $\mathbf{C}(s)$ for a plant $\mathbf{G}_n(s)$ the so-called mixed sensitivity problem has to be solved (Skogestad and Postlethwaite 2005). A controller is derived in such a way that a compromise between robust stability, disturbance rejection and spent energy is obtained. Hence, both stability and performance are addressed. To define the individual requirements for the closed-loop sensitivity $\mathbf{S}(s) = (\mathbf{I} + \mathbf{G}_n(s)\mathbf{C}(s))^{-1}$ related to the performance of the loop, for the restriction of the magnitude of the plant input, described by $\mathbf{C}(s)\,\mathbf{S}(s)$, and robustness related to the complementary sensitivity function $\mathbf{T}(s) = (\mathbf{I} + \mathbf{G}_n(s)\mathbf{C}(s))^{-1}\mathbf{G}_n(s)\mathbf{C}(s)$, frequency dependent weights, $\mathbf{W}_s(s)$, $\mathbf{W}_{cs}(s)$, $\mathbf{W}_T(s)$ have to be chosen. The selected MIMO-weights are diagonal matrices for which reason the maximal and minimal singular values coincide, see Figure 15.

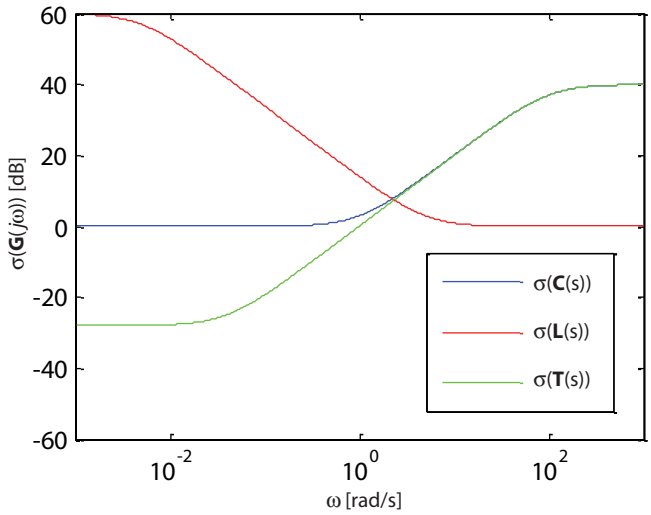

Figure 15. MIMO-weights of the mixed-sensitivity problem.

The selected sensitivity weight $\boldsymbol{W}_S(s)$ addresses good disturbance attenuation while a value of 0 dB in the lower frequency range for the weight of the complementary sensitivity $\mathbf{W}_T(s)$ indicates good setpoint tracking. By the choice of $\mathbf{W}_{CS}(s)$ actuation is promoted in the lower frequency range, while high frequency actuation is avoided by high penalties. However, shaping the desired closed-loop behaviour in this way is limited. The sensitivity $\mathbf{S}(s)$ and the complementary sensitivity $\mathbf{T}(s)$ are not independent from each other, but fulfil $\mathbf{S} + \mathbf{T} = \mathbf{I}$ for all frequencies.

The optimal controller $\mathbf{C}(s)$ is calculated by H_∞-minimization (Kwakernaak 1993). The weight matrices $\mathbf{W}_T(s)$, $\mathbf{W}_{CS}(s)$, $\mathbf{W}_S(s)$ are combined to a cost function $\mathbf{N}(\mathbf{C}_S(s))$ which is minimized over all stabilizing controllers $\mathbf{C}(s)$:

$$\min_C \left\| \mathbf{N}(\mathbf{C}(s)) \right\|_\infty, \quad \mathbf{N} = \begin{bmatrix} \mathbf{W}_T(s)\mathbf{T}(s) \\ \mathbf{W}_{cs}(s)\mathbf{C}(s)\mathbf{S}(s) \\ \mathbf{W}_s(s)\mathbf{S}(s) \end{bmatrix} \tag{7}$$

Results for the synthesized controller $\mathbf{C(s)}$ and the resulting singular values for the open-loop, sensitivity, and complementary sensitivity are given in Figure 16. The obtained $\mathbf{T}(s)$ in black colour indicates a satisfactory setpoint tracking, the ratio between the given reference and the output equals 0 dB, that equates to a ratio of 1:1. This is corroborated by low values of the sensitivity $\mathbf{S}(s)$ implying a good disturbance attenuation for low frequencies as well. The bandwidth of the frequency response of the open-loop function $\mathbf{L}(s)$ indicates little acceleration compared to the nominal model.

4. RESULTS

For the investigation of the presented control approaches wind tunnel experiments are conducted at a Reynolds number of $Re = 840000$. The goal is to influence the vortex structures near the side-walls and the separated flow above the blade simultaneously and thereby stabilize the system throughout the

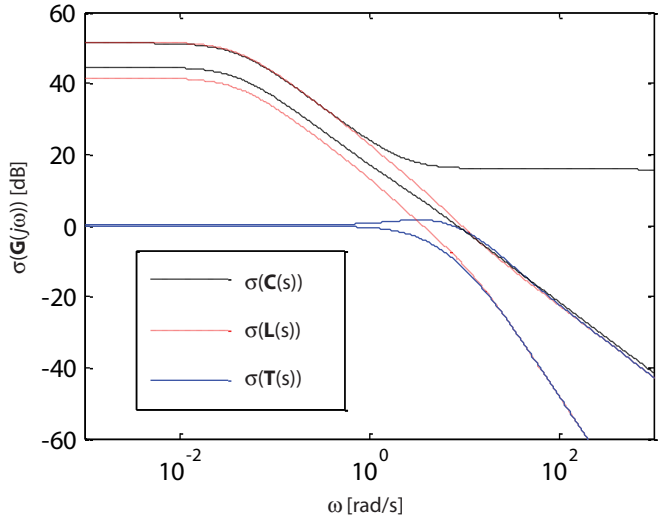

Figure 16. Singular values of the H_∞-controller **C**(*s*), the open loop transfer function **L**(*s*) and the complementary sensitivity **T**(*s*).

whole operating range. In a first step, both control variables are supposed to follow different reference commands at the same time. Next, the system is disturbed intensely. With that the robustness of the proposed closed-loop control is tested experimentally. Only when the applied control law is capable of compensating heavy disturbances in a fast manner it has the potential to guarantee safe operating conditions in real flight situations in the future.

To simulate disturbances, the deflection angle of the compressor cascade can be shifted quickly. Through a higher turning angle the pressure at the trailing edge rises. Concomitantly, the risk of flow separation increases. Moreover, the pressure induced boundary separation on the suction side occurs further upstream and the corner vortices extend further towards mid-span.

In contrast to that a decrease of the deflection angle results in a reduction in pressure at the trailing edge and the corner vortices stay closer to the sidewalls. The effects of a change in the deflection angle of the compressor cascade on both control variables are presented in Figure 17 for the case with and without ($p_d = 0$) actuation. The design case is given by $\beta = 60°$.

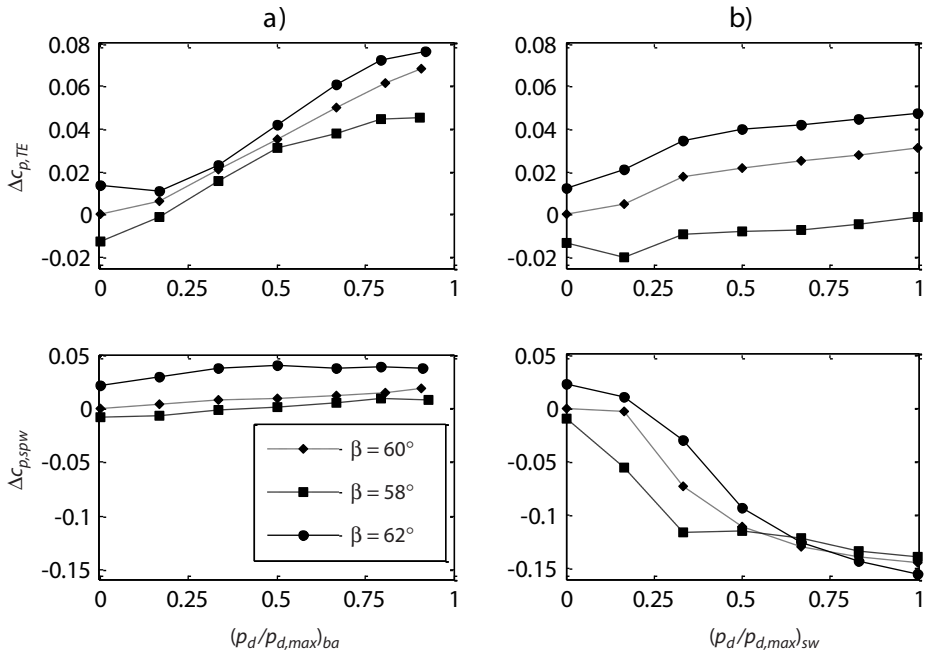

Figure 17. Influence of angle distortions on the control variables.

In the upper plot in Figure 17 a) it can be seen that a change in the deflection angle of $\Delta\beta = -2°$ leads to a loss of pressure at the trailing edge of $\Delta c_{p,TE} = -0.013$ in the case without actuation. At this turning angle a maximal pressure rise of $\Delta c_{p,TE} = 0.04$ is attainable with the maximal amplitude of the blade actuators. Similar conclusions can be drawn from the other three plots in Figure 17.

Generally, the nonlinear characteristics seen are an indication of the complex flow field within the cascade. However, regarding Figure 17, it has to be marked that for the base flow situation, the inlet flow conditions are hold homogeneously by an elaborate adjustment of the boundary layer suction. Under disturbed circumstances this is no longer the case. A new adjustment is not deemed to be necessary as a closed-loop control experiment is applied anyway. In real flight situations the controller has to compensate such disturbances. Hence, this fact can be regarded as an additional challenge for the controller.

The result of a MIMO-control experiment with the proposed inverse-based controller is shown in Figure 18. On the left the measured values of the control variables are given. Both process variables are supposed to follow a series of step commands $r(t)$, each one lasting for ten seconds. On the upper right hand side the corresponding values of the actuation variables can be seen, respectively. Starting from t = 50 s to t = 80 s the reference command is held constant and a disturbance is simulated by shifting the deflection angle β quickly.

Comparing the control variables with the given reference commands, both outputs demonstrate a satisfying behaviour. Neither constant errors nor overshooting responses appear. Moreover, the demands regarding $\Delta c_{p,spw}$ can be achieved significantly faster than those concerning $\Delta c_{p,TE}$. In the first case the settling time to reach a new constant value in the mean is less than half a second, in the latter case about double of this time is necessary.

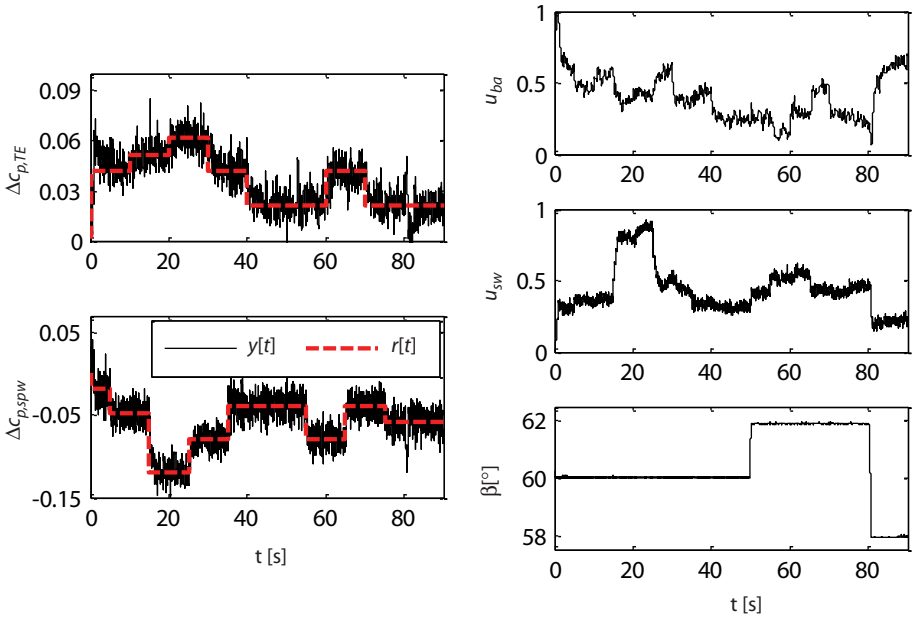

Figure 18. Results obtained with an IBC.

A first disturbance is introduced at t = 50 s by increasing the turning angle to $\beta = 62°$. Here the coupling of the flow structures becomes obvious. The higher deflection angle leads to a stronger development of the corner vortices. Therefore the actuators at the sidewall have to react and the value of u_{sw} rises. Concomitantly, the pressure at the trailing edge $c_{p,TE}$ increases and the amplitude of the blade actuators u_{ba} can be reduced. Generally, it is noticeable that this disturbance has a rather weak impact on the flow condition and can be compensated for completely and quickly. Yet, the next disturbance at t = 80 s of $\Delta\beta = -4°$ shows obviously a much stronger effect. At a deflection angle of $\beta = 58°$ the secondary flow structures develop less strongly and the interference of the sidewall actuators is reduced significantly. As a consequence of the changed flow conditions and the reduced sidewall actuation, the amplitude of u_{ba} has to be tripled in order to obtain the desired reference command. Thus, the second disturbance can be rejected as well, but more time is needed compared to the first one.

After this successful primary test, the controller is challenged further. In the following experiment the introduced disturbances are intensified substantially. Here, a continuous increase of the pressure at the trailing edge $c_{p,TE}$ and stronger pushing of the corner vortices towards the side-walls are required as indicated by the reference commands given in Figure 19. At the same time disturbances are introduced every ten seconds changing the deflection angle β.

The first disturbance at t = 5 s leads to a significant decrease of $c_{p,TE}$. To achieve the desired reference command concerning $\Delta c_{p,spw}$ at a lower deflection angle of β = 58° the amplitude of the sidewall actuators has to be reduced to almost zero. Consequently the influence of the blade actuators has to be increased significantly in order to reach the desired pressure value. While the effect of the disturbance concerning $\Delta c_{p,spw}$ can be compensated for quickly, nearly 3.5 s are necessary to drive the system back to the reference value of $\Delta c_{p,TE}$. In contrast, the disturbance at t = 15 s to a deflection angle of β = 62°, results in a strong increase of pressure rise at the trailing edge. Therefore, the blade actuators no longer have to control the flow. By enhancing the turning angle the corner vortices extend so that the sidewall actuators have to force strongly. This time the impact of the sidewall actuators is already sufficient to obtain the desired value of $\Delta c_{p,TE}$. For the step commands between t = 30 s and t = 60 s an almost similar behaviour can be seen.

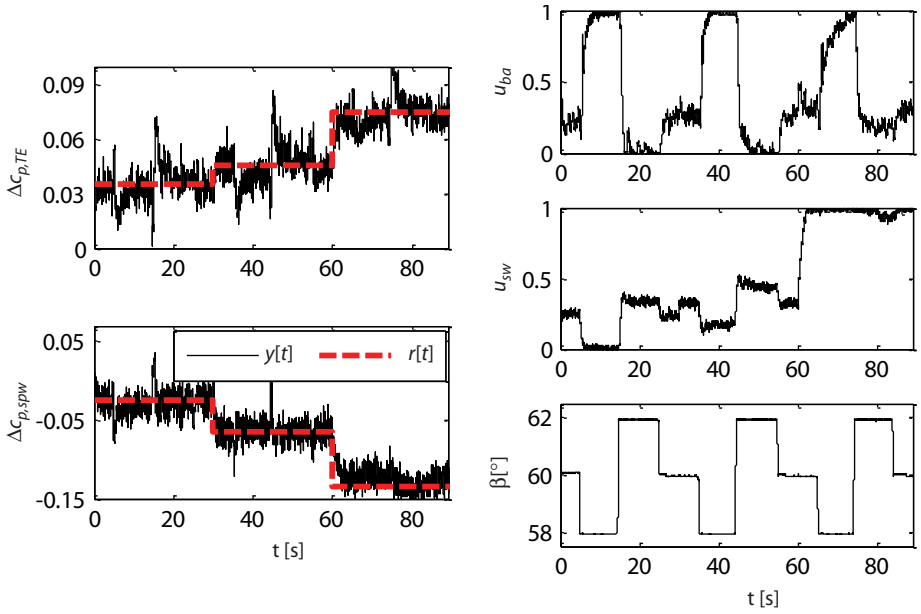

Figure 19. Results obtained with an IBC under heavy inlet angle distortions.

Within the period of the last reference command between t = 60 s and t = 90 s an interesting phenomenon occurs. Due to the very low required value of $\Delta c_{p,spw}$ the amplitude of u_{sw} becomes maximal. Even a reduction of the deflection angle down to β = 58° at t = 65 s releases the sidewall actuators only marginally. At t = 75 s the turning angle is increased by $\Delta\beta$ = +4° and a nonlinear effect is observable. Due to the higher deflection the amplitude of the blade actuator can be diminished as expected. Surprisingly the amplitude u_{sw} decreases as well. Before, the negative effect of the blade actuators upon the spanwise pressure difference $\Delta c_{p,spw}$ was negligible. However, at the considered operating point this is no longer valid.

Yet, it can be concluded that all set reference commands are obtained even under the influence of heavy inlet angle distortions. For this, a partly strong forcing of the actuation is necessary. The control of the local control variable $\Delta c_{p,spw}$ can be realized faster than of the global variable $\Delta c_{p,TE}$.

Next, the multivariable H_∞-control approach is tested and an almost identical experiment to that in Figure 19 is conducted to challenge the controller, see Figure 20. Again the requirements are increased during the experiment while disturbing the process intensely every ten seconds.

The observable setpoint tracking is almost as good as the one received with the previous IBC. However, small constant errors occur. This is due to the fact that for the solution of the mixed-sensitivity problem, cf. Chapter 3.3, only asymptotically stable weights can be taken into account. As

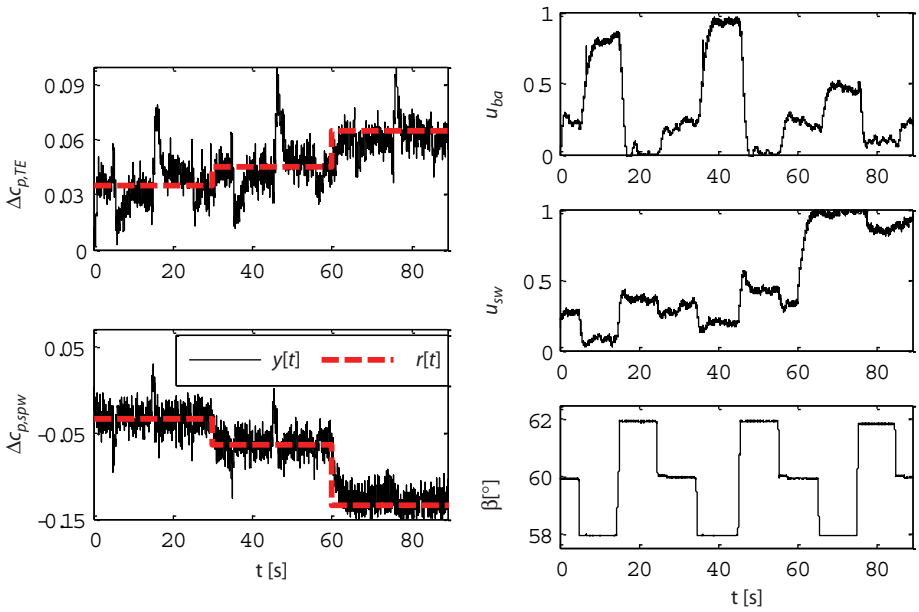

Figure 20. Experimental results obtained with a H_∞-controller under the influence of heavy inlet angle distortions.

a result the values of $\mathbf{W}_S(s)$ in the lower frequency range are limited and an absolute integrating control behaviour, leading to a disappearing tracking error, is not possible. Apart from that no overshoots occur and all disturbances can be compensated.

As discussed above the robust controller guarantees stability over all identified models of the model family Π (Hecklau et al., 2010a), (Wiederhold, et al. 2010). Hence, the controller is designed in a more conservative fashion and the performance is lower than that of the IBC. Nevertheless, this difference is small.

In total, the two presented MIMO-control approaches satisfy the required demands. Either controller is capable to obtain a good setpoint tracking. Moreover, both strategies are able to react upon intense disturbances immediately and compensate their outcomes. Finally closed-loop control provides the capability to adapt the amount of actuation energy needed down to a minimum in response to the actual operating point.

5. CONCLUSION AND OUTLOOK

The presented work shows a successful application of two multivariable controllers at a highly loaded compressor cascade. By application of active flow control a rise in pressure of more than 10% is attainable in the chosen setup with less than 0.5% of the passage mass flow as actuator input.

It is demonstrated that a critical turning of the flow is realizable by application of active flow control. The proposed control algorithms are capable of driving the system to desired operating points. Even under the influence of heavy disturbances the closed-loop controllers can guarantee stable operating conditions. Flow separation can be avoided or at least mitigated. The pressure induced boundary layer separation on the suction side of a cascade blade in the rear part can be significantly reduced. Moreover, the blockade of the passage mean flow can be diminished by pulsed blowing out of the sidewall. Accordingly, the realizable pressure gain of the compressor cascade can be enhanced at a critical deflection angle. Furthermore, closed-loop control is shown to adapt the actuation energy down to a necessary level so that an energy waste is prevented. To the authors' knowledge this is the first application of multivariable closed-loop controllers in a stator cascade where the interference occurs at the shear-layer level.

With the application of multivariable control methods a simultaneous manipulation of the dominant coupled flow structures is possible. A robust H_∞-controller guarantees stability over all identified plant models. Moreover, a classical inverse-based controller enables the decoupled influence of both dominant separation phenomena at the same time.

The present investigation shows the potential of closed-loop control to contribute to the continuous improvement in turbomachine technology. For higher Mach numbers, the relevant time scales decrease drastically. It remains part of ongoing research at the Berlin Institute of Technology to scale the solution up to a configuration which is run at a Mach number of 0.7. According to our estimation the main limiter of AFC within turbomachines that run at high Mach numbers will primarily be the applied actuators. To rise the bandwidth of the applied controller is not a problem from the present point of view.

ACKNOWLEDGMENTS

This work is funded by the "Deutsche Forschungsgemeinschaft" (DFG) and the industrial partner Rolls Royce Deutschland as a part of the transfer project: "DFG-TFB Rolls Royce: Smart Active Control for Turbomachinery Blades".

REFERENCES

[I] Beaudoin, J. F., O. Cadot, J.-L. Aider, and J.-E. Wesfreid. "Drag reductions of a bluff body using adaptive control methods." *Phys. of Fluids* 18: 1-10, 2006.

[2] Burgmann, S., and W. Schröder. "Investigation of the vortex induced unsteadiness of a separation bubble via time-resolved and scanning PIV measurements." Exp. Fluids 45: 675691, doi 10.1007/s00348-008-0548-7, 2008.

[3] Culley, D. E., M. M. Bright, P. S. Prahst, and A. J. Strazisar. "Active flow separation control of a stator vane using surface injection in a multistage compressor experiment." *J. Turbomach.* 126: 24-35, 2004.

[4] Day, I. J., T. Breuer, J. Escuret, M. Cherret, and A. Wilson. "Stall inception and the prospects for active control in four high-speed compressors." *J. Turbomach.* 121: 18-27, 1999.

[5] Epstein, A. H., J. E. Ffowcs Williams, and E. M. Greitzer. "Active suppression of aerodynamic instabilities in turbomachines." *J. of Propulsion and Power* 5: 204-211, 1989.

[6] Eveker, K. M., D. L. Gysling, C. N. Nett, and O. P. Sharma. "Integrated control of rotating stall and surge in high-speed multistage compression systems." *J. Turbomach.* 120: 440-445, 1998.

[7] Fiedler, H., and H. Fernholz. "On the management and control of turbulent shear flows." *Prog. Aerospace Sci.* 27: 305-387, 1990.

[8] Gad-el-Hak, M., A. Pollard, and J.-P. Bonnet. *Flow control: Fundamentals and practices*. Berlin: Springer-Verlag, 1998.

[9] Gmelin, C., M. Steger, E. Wassen, F. Thiele, A. Huppertz, and M. Swoboda. URANS simulations of active flow control on highly loaded turbomachinery blades. In: King, R. (Editor): Active Flow Control II, Notes on Numerical Fluid Mechanics and Multidisciplinary Design, Vol. 108, Berlin Heidelberg: Springer-Verlag, 203 - 219, 2010.

[10] Hecklau, M., O. Wiederhold, V. Zander, R. King, W. Nitsche, and M. Swoboda. "Active separation control with pulsed jets in a critically loaded compressor cascade." *AIAA 5th Flow Control Conference*. AIAA 2010-4252. Chicago, U.S.A., 2010a.

[11] Hecklau, M., V. Zander, I. Peltzer, W. Nitsche, A. Huppertz, and M. Swoboda. *Experimental AFC approaches on a highly loaded compressor cascade*. In: King, R. (Editor): *Active Flow Control II,* Notes on Numerical Fluid Mechanics and Multidisciplinary Design, Vol. 108, Berlin Heidelberg: Springer-Verlag, 171 - 186, 2010b.

[12] Hecklau, M., R. van Rennings, V. Zander, W. Nitsche, A. Huppertz, and M. Swoboda. "Particle image velocimetry of active flow control on a compressor cascade." *Exp. Fluids,* doi.org/10.1007/s00348-010-0895-z, 2010c.

[13] Heinz, N., Haucke, F., King, R., and W. Nitsche. "Robust Closed-Loop Control on a 2D-High-Lift-Device." *Int. J. Flow Contr.* 2: 91 - 108, 2010.

[14] Inoue, M., and M. Kuroumaru. "Structure of tip clearance flow in an isolated axial compressor rotor." *J. Turbomach.* 111: 250 - 256, 1989.

[15] Kwakernaak, H. "Robust control and H_m-optimization - tutorial paper." *Automatica* 29: 255273, 1993.

[16] Kwakernaak, H. "Robustness optimization of linear feedback systems." *Preprints 22nd IEEE Conf. on Decision and Contr.* San Antonio, U.S.A., 1983. [17] Langston, L. S. "Crossflows in a turbine cascade passage." *J. Eng. Power* 102: 866 - 874, 1980.

[18] Lord, W. K., D. G. MacMartin, and G. Tillmann. "Flow Control Opportunities in Gas Turbine engines." *AIAA Flow Control Conference*. AIAA 2000-2234. Denver, U.S.A., 2000.

[19] McLean, J., J. Crouch, R. Stoner, S. Sakurai, G. Seidel, W. Feifel, and H. Rush. "Study of the application of separation control by unsteady excitation to civil transport aircraft." Technical Report NASA/CR 1999-209338, Langley Research Center, Hampton, Virginia, U.S.A., 1999.

[20] Mertens, D., F. Thiele, M. Swoboda, and A. Huppertz. „Transition modeling effects on the simulation of a stator cascade with active flow control." ASME Turbo Expo. GT2008-50697. Berlin, Germany, 2008.

[21] Nelson, E. B., J. D. Paduano, and A. H. Epstein. "Active stabilization of surge in an axicentrifugal turboshaft engine." *J. Turbomach*. 122: 485-493, 2000.

[22] Nerger, D., H. Saathoff, and R. Radespiel. "Experimental and numerical analysis of a highly loaded low aspect ration compressor stator cascade." *7th European Turbomachinery Conference*. Athen, Greece, 2007.

[23] Paschereit, C. O., E. Gutmark, and W. Weisenstein. "Excitation of thermoacoustic instabilities by the interaction of acoustics and unstable swirling flow." *AIAA Journal* 38: 1025-1034, 2000.

[24] Skogestad, S., and I. Postlethwaite. *Mulivariable feedback control*. John Wiley & Sons, 2005.

[25] Tavakoli, S., I. Griffin, and P. Fleming. "An overview of compressor instabilities: basic concepts and control." *Proceedings of the 16th IFAC International Symposium on Automatic Control in Aerospace*. St. Petersburg, Russia, 2004.

[26] The MathWorks, Inc. "MATLAB - System identification toolbox, user's guide." Nantucket, MA, U.S.A., 1997.

[27] Walsh, P. P., and P. Fletcher. *Gas Turbine Performance*. UK: Blackwell Science, 1998.

[28] Weigl, H. J., and J. D. Paduano. "Application of H_∞-control with eigenvalue perturbations to stabilize a transonic compressor." *Proceedings of the 1997 Conference on Control Applications*. Hartford, U.S.A., 1997.

[30] Wiederhold, O., R. King, and B. R. Noack. *Robust control in turbomachinery configurations*. In: King, R. (Editor): *Active Flow Control II,* Notes on Numerical Fluid Mechanics and Multidisciplinary Design, Vol. 108, Berlin Heidelberg: Springer-Verlag, 187 - 202, 2010.

[31] Zander, V., M. Hecklau, W. Nitsche, and I. Peltzer. "Active control of corner vortices on a highly loaded compressor cascade." *8th European Turbomachinery Conference*. Graz, Austria, 2009.

[32] Zhu, Y. *Multivariable system identification: for process control*. Oxford: Elsevier Science Ltd., 2001.